Zeolite Synthesis Using Flexible Diquaternary Alkylammonium Ions $(C_nH_{2n+1})_2HN^+(CH_2)_5N^+H(C_nH_{2n+1})_2$ with $n = 1-5$ as Structure-Directing Agents

Bada Han,[†] Song-Ho Lee,[†] Chae-Ho Shin,[‡] Paul A. Cox,[§] and Suk Bong Hong*,[†]

Division of Chemical Engineering, Hanbat National University, Taejon 305-719, Korea, Department of Chemical Engineering, Chungbuk National University, Chungbuk 361-763, Korea, and School of Pharmacy and Biomedical Science, University of Portsmouth, Portsmouth PO1 2DT, United Kingdom

Received September 14, 2004. Revised Manuscript Received November 10, 2004

The use of a series of flexible, linear diquaternary alkylammonium ions $(C_nH_{2n+1})_2HN^+(CH_2)_5N^+H(C_nH_{2n+1})_2$ with $n = 1-5$ as structure-directing agents in zeolite syntheses is described. Among the ammonium ions studied here, the $(CH_3)_2HN^+(CH_2)_5N^+H(CH_3)_2$ and $[(CH_3)_2CH]_2HN^+(CH_2)_5N^+H[CH(CH_3)_2]_2$ ions were found to be new structure-directing agents for the crystallization of levyne and MCM-22, respectively. The overall synthesis results of this study reveal that the phase selectivity of the crystallization can differ according to both the length of the dialkyl substituents on the ammonium ion and the oxide composition of synthesis mixtures. The host−guest interactions in nonasil, ZSM-12, mordenite, and levyne containing $(CH_3)_2HN^+(CH_2)_5N^+H(CH_3)_2$ as a guest molecule are investigated by $^1H-^{13}C$ CP MAS NMR and Raman spectroscopies, and computer modeling studies, and it is shown that the organic guest molecules adopt distinct conformations in order to fit in the pores of each zeolite host.

Introduction

Since the pioneering work by Barrer in the early 1960s,[1] a wide variety of organic additives, usually referred to as structure-directing agents (SDAs), has been extensively used in the hunt for novel zeolites and related microporous materials.[2] Whereas the conformational rigidity and hydrophobicity of these organic SDAs are believed to be the two most important factors determining the pore architecture of the crystallized product,[3] the essentially opposite strategy, which includes the use of organic species with a high degree of flexibility and charge density, has also led to the discovery of previously unobserved framework topologies. A successful example of the latter approach is the linear diquaternary ion $(C_2H_5)_3N^+(CH_2)_5N^+(C_2H_5)_3$ (*N*,*N*′-bis-triethylpentanediyldiammonium, Et_6-diquat-5), because this flexible cation is the only known SDA leading to the formation of ZSM-57 (MFS) with the intersecting 10- and 8-ring pore system.[4,5]

A recent series of our studies on zeolite syntheses in the presence of $(C_2H_5)_3N^+(CH_2)_n-N^+(C_2H_5)_3$ ions (Et_6-diquat-*n* with $n = 3-10$) has shown that Et_6-diquat-5 can produce another three different zeolites (i.e., P1 (GIS), SSZ-16 (AFX), and SUZ-4), as well as ZSM-57, depending on the oxide composition of synthesis mixtures.[6−9] However, no zeolitic phases other than ZSM-5 (MFI), mordenite (MOR), and analcime (ANA), which are known to crystallize in the absence of organic SDA,[2] were obtained from syntheses using the other seven organic SDAs with two triethylammonium groups. A similar trend has also been observed for zeolite syntheses using a series of $(CH_3)_3N^+(CH_2)_nN^+(CH_3)_3$ ions (Me_6-diquat-*n* with $n = 3-10$): Me_6-diquat-5 can direct the synthesis of at least four different zeolite structures including EU-1 (EUO), ZSM-48, ZSM-12 (MTW), and MCM-22 (MWW), displaying the most diverse phase selectivity with respect to the gel composition among the eight diquaternary cations with different central chain lengths.[10,11] An interesting result is that neither of the zeolites prepared with Me_6-diquat-5 has the same framework topology as that of any of the materials that can be synthesized using Et_6-diquat-5. This implies that the phase selectivity of the crystallization in the presence of flexible diquaternary ions with the general formula $R_3N^+(CH_2)_nN^+R_3$ can be notably altered according to the length of the groups on the ammonium ion, as well as to that of the central alkyl chain, although the structure-directing abilities of these organic species are not strong enough to dominate over the impact of inorganic gel chemistry.[9,11]

The present study focuses on the use of another series of linear diquaternary ammonium ions, i.e., $(C_nH_{2n+1})_2HN^+(CH_2)_5N^+H(C_nH_{2n+1})_2$ with $n = 1-5$, which are formed of

* To whom correspondence should be addressed. Tel: +82-42-821-1549. Fax: +82-42-821-1593. E-mail: sbhong@hanbat.ac.kr.
[†] Hanbat National University.
[‡] Chungbuk National University.
[§] University of Portsmouth.

(1) Barrer, R. M.; Denny, P. J. *J. Chem. Soc.* **1961**, 971.
(2) Szostak, R. *Handbook of Molecular Sieves*; Van Nostrand Reinhold: New York, 1992.
(3) Lobo, R. F.; Zones, S. I.; Davis, M. E. *J. Inclusion Phenom. Mol. Recognit. Chem.* **1995**, *21*, 47.
(4) Valyocsik, E. W.; Page, N. M. Eur. Pat. Appl. 174,121, 1986.
(5) Schlenker, J. L.; Higgins, J. B.; Valyoscik, E. W. *Zeolites* **1990**, *10*, 293.
(6) Paik, W. C.; Shin, C.-H.; Hong, S. B. *Chem. Commun.* **2000**, 1609.
(7) Lee, S.-H.; Lee, D.-K.; Shin, C.-H.; Paik, W. C.; Lee, W. M.; Hong, S. B. *J. Catal.* **2000**, *196*, 158.
(8) Paik, W. C.; Shin, C.-H.; Lee, J. M.; Ahn, B. J.; Hong, S. B. *J. Phys. Chem. B* **2001**, *105*, 9994.
(9) Lee, S.-H.; Shin, C.-H.; Choi, G. J.; Park, T.-J.; Nam, I.-S.; Han, B.; Hong, S. B. *Microporous Mesoporous Mater.* **2003**, *60*, 237.
(10) Lee, S.-H.; Shin, C.-H.; Hong, S. B. *Chem. Lett.* **2003**, *32*, 542.
(11) Lee, S.-H.; Shin, C.-H.; Yang, D.-K.; Ahn, S.-D.; Nam, I.-S.; Hong, S. B. *Microporous Mesoporous Mater.* **2004**, *68*, 97.

10.1021/cm048418+ CCC: $30.25
Published on Web 01/07/2005

two dialkylammonium groups connected by a pentamethylene bridging unit, as organic SDAs in zeolite syntheses. Here we show that among the diquaternary cations studied here, the $(CH_3)_2HN^+(CH_2)_5N^+H(CH_3)_2$ (*N*,*N*′-bis-dimethylpentanediyldiammonium, Me_4-diquat-5) and $[(CH_3)_2CH]_2HN^+(CH_2)_5N^+H[CH(CH_3)_2]_2$ (*N*,*N*′-bis-diisopropylpentanediyldiammonium, *iso*-Pr_4-diquat-5) ions can produce levyne (LEV) and MCM-22, respectively, when the concentrations of Al and NaOH in the gel are properly selected. To our knowledge, all the synthesis routes to LEV-type microporous materials published thus far share in common the use of polycyclic organic species such as 1-adamantanamine, *N*-methylquinuclidinium iodide, or tropine,[12−17] whose shapes and sizes are notably different from those of Me_4-diquat-5. In addition, none of the aliphatic organic SDAs, with the exception of Me_6-diquat-5,[10] have been reported to direct the synthesis of MWW-type zeolites.[18−20] The materials prepared in this study are characterized by using different techniques including powder X-ray diffraction, elemental and thermal analyses, scanning electron microscopy, Raman, $^1H-^{13}C$ CP MAS NMR, and computer modeling studies.

Experimental Section

Synthesis. The Me_4-diquat-5 cation was prepared by refluxing 1,5-dibromopentane (97%, Aldrich) with an excess of dimethylamine (2.0 M solution in tetrahydrofuran (THF), Aldrich) in THF as a solvent overnight. The excess amine was removed by extraction with THF and recrystallizations were performed in methanol−diethyl ether mixtures. The other seven divalent cations (i.e., Et_4-diquat-5, Pr_4-diquat-5, *iso*-Pr_4-diquat-5, Bu_4-diquat-5, *iso*-Bu_4-diquat-5, Pe_4-diquat-5, and *sec*-Bu_4-diquat-5) were synthesized using the corresponding dialkylamines instead of dimethylamine, respectively, with procedures similar to the Me_4-diquat-5 preparation. After purification, the formation and purity of all these diquaternary ammonium salts were confirmed by ^1H and ^{13}C NMR.

The reagents used for zeolite syntheses included NaOH (50% aqueous solution, Aldrich), diquaternary cations prepared here, $Al(NO_3)_3 \cdot 9H_2O$ (98%, Junsei), fumed silica (Aerosil 200, Degussa), and deionized water. The final composition of the synthesis mixture was $3.0(C_nH_{2n+1})_4$-diquat-5$\cdot x Na_2O \cdot y Al_2O_3 \cdot 30SiO_2 \cdot 1200H_2O$, where x and y are varied between $3.0 \le x \le 17.0$ and $0.0 \le y \le 1.0$, respectively. After stirring at room temperature for 24 h, the synthesis mixture was charged into Teflon-lined 23-mL autoclaves and heated to 433 K under rotation (100 rpm) for 1−14 days. The solid products were recovered by filtration, washed repeatedly with water, and then dried overnight at room temperature. To obtain their proton form, when necessary, as-made zeolites were calcined under flowing air at 823 K for 8 h and refluxed twice in 1.0 M NH_4NO_3 solutions for 6 h followed by calcinations at 773 K for 4 h.

Analytical Methods. The phase purity and crystallinity were determined by powder X-ray diffraction (XRD) using a Rigaku Miniflex or 2500H diffractometer with Cu Kα radiation. Chemical analysis for Si, Al, and Na was carried out by a Jarrell-Ash Polyscan 61E inductively coupled plasma (ICP) spectrometer in combination with a Perkin-Elmer 5000 atomic absorption spectrophotometer. The C, H, and N contents of selected samples were analyzed by using a Carlo Erba 1106 elemental organic analyzer. Thermogravimetric analyses (TGA) were performed in air on a TA Instruments SDT 2960 thermal analyzer, where the exothermic weight loss related to the combustion of organic SDA was further confirmed by differential thermal analyses (DTA) using the same analyzer. Crystal morphology and size were determined by a JEOL JSM-6300 scanning electron microscope (SEM). The N_2 sorption experiments were performed on a Micromeritics ASAP 2010 analyzer.

The ^{27}Al MAS NMR spectra at a spinning rate of 11.0 kHz were recorded on a Bruker Avance 500 spectrometer with a 4-mm double-resonance Bruker MAS probe. The operating ^{27}Al frequency was 130.336 MHz, and the spectra were obtained with an acquisition of about 1000 pulse transients, which were repeated with a $\pi/20$ rad pulse length of 0.5 μs and a recycle delay of 1 s. The ^{27}Al chemical shifts are referenced to an $Al(H_2O)_6^{3+}$ solution. Spectral deconvolution and simulation were performed using the PeakFit curve-fitting program. The $^1H-^{13}C$ CP MAS NMR spectra at a spinning rate of 4.5 kHz were recorded on the same spectrometer at a ^{13}C frequency of 125.779 MHz with a $\pi/2$ rad pulse length of 5.0 μs, a contact time of 1 ms, and a recycle delay of 5 s. Approximately 5000 scans were accumulated. The ^{13}C chemical shifts are reported relative to TMS. The Raman spectra were recorded on a Bruker RFA 106/S FT-Raman spectrometer equipped with an Nd:YAG laser operating at 1064 nm. The samples were exposed to a laser power of 100−250 mW at the spectral resolution of 4 cm^{-1}. Typically, 400−1600 scans were accumulated for obtaining the Raman spectra.

Computer simulation of the energy-minimized locations and conformations of organic SDAs occluded within the pores of zeolites prepared here was carried out using a combined Monte Carlo−Simulated Annealing (MC−SA) approach.[21] Calculations were performed using the CVFF force field as implemented in the program Discover,[22] as described in our recent work.[23] The host zeolite lattice was held fixed during the simulation, while the organic SDA occluded was free to move. The unit cell parameters and atomic coordinates for zeolites under computer simulation were taken from the original references listed in the International Zeolite Association (IZA) tabulations,[24] and their frameworks were modeled as pure silica structures. During the initial Monte Carlo stage of the calculation, the configuration of the diquaternary cation was accepted only if the calculated energy was below 4200 kJ·mol^{-1}, otherwise the process was started again. Once an initial configuration had been accepted, successive molecular dynamics simulations were carried out at 1000, 750, 500, 300, 200, 100, and 50 K for 1000 time steps of 1 fs at each temperature, prior to a final energy minimization stage.

Results and Discussion

Table 1 lists the representative products from syntheses using each of $(C_nH_{2n+1})_4$-diquat-5 series as an organic SDA

(12) McCusker, L. B. *Mater. Sci. Forum* **1993**, *133−136*, 423.
(13) Kerr, G. T. U.S. Patent 3,459,676, 1969.
(14) Cannan, T. R.; Brent, M. T.; Flanigen, E. M. Eur. Pat. Appl. 91,048 A1, 1983.
(15) Zhu, G.; Xiao, F.-S.; Qiu, S.; Hun, P.-C.; Xu, R.; Ma, S.; Terasaki, O. *Microporous Mesoporous Mater.* **1997**, *11*, 269.
(16) Millini, R.; Carati, A.; Bellussi, G. *Zeolites* **1992**, *12*, 265.
(17) Barrett, P. A.; Jones, R. H.; Sankar, G.; Thomas, J. M.; Shannon, I. D.; Catlow, C. R. *J. Chem. Soc., Chem. Commun.* **1996**, 2001.
(18) Puppe, L.; Weisser, J. U.S. Patent 4,439,409, 1984.
(19) Zones, S. I. Eur. Pat. Appl. 231,860, 1987.
(20) Bellusi, G.; Perego, G.; Clerici, M. G.; Giusti, A. Eur. Pat. Appl. 293,-032, 1988.
(21) Stevens, A. P.; Gorman, A. M.; Freeman, C. M.; Cox, P. A. *J. Chem. Soc., Faraday Trans.* **1996**, *92*, 2065.
(22) *Discover*, version 99.1; Accelrys: San Diego, CA.
(23) Hong, S. B.; Lear, E. G.; Wright, P. A.; Zhou, W.; Cox, P. A.; Shin, C.-H.; Park, J.-H.; Nam, I.-S. *J. Am. Chem. Soc.* **2004**, *126*, 5817.
(24) Treacy, M. M. J.; Higgins, J. B.; von Ballmoos, R. *Collection of Simulated XRD Patterns for Zeolites*; Elsevier: London, 1996.

Table 1. Syntheses from Gel Composition $3.0R{\cdot}xNa_2O{\cdot}yAl_2O_3{\cdot}30SiO_2{\cdot}1200H_2O$[a,b]

	$x = 5.0$				$x = 9.0$			
	SiO_2/Al_2O_3 ratio in the synthesis mixture				SiO_2/Al_2O_3 ratio in the synthesis mixture			
organic SDA	30	60	120	∞	30	60	120	∞
Me_4-diquat-5	amorphous[c]	nonasil	ZSM-12	nonasil	amorphous	D + (mordenite)	D + nonasil	L
Et_4-diquat-5	amorphous[c]	ZSM-5	D + ZSM-5	D	mordenite	mordenite	L	L
Pr_4-diquat-5	amorphous[c]	ZSM-5	ZSM-5	ZSM-5	ZSM-5	ZSM-5	ZSM-5	ZSM-5
iso-Pr_4-diquat-5	amorphous[c]	amorphous	amorphous	D	MCM-22	ferrierite + (D)	L + D	L + D
Bu_4-diquat-5	amorphous[c]	ZSM-11/ZSM-5	ZSM-11/ZSM-5	ZSM-5[d]	mordenite	ZSM-5	ZSM-5	D
iso-Bu_4-diquat-5	amorphous[c]	amorphous	amorphous	amorphous	amorphous	D + (mordenite)	D + (mordenite)	D
Pe_4-diquat-5	amorphous[c]	ZSM-11/ZSM-5	ZSM-11/ZSM-5	ZSM-5[d]	ZSM-5	ZSM-5	D + ZSM-5	D
sec-Bu_4-diquat-5	amorphous[c]	amorphous	ZSM-11/ZSM-5	D	amorphous	ZSM-5 + mordenite	D + ZSM-5	D

[a] R is organic SDA and y is varied between $0 \le y \le 1.0$. Crystallization was performed under rotation (100 rpm) at 433 K for 7 days, unless otherwise stated. [b] Final products are given in decreasing order of relative abundance based on powder XRD, and the phase obtained in a trace amount is given in parentheses. D and L are dense (mainly quartz) and layered phases, respectively. [c] The material obtained after 14 days of heating at 433 K. [d] The material obtained after 3 days of heating at 433 K.

and aluminosilicate gels in which the SiO_2/Al_2O_3 ratio is varied from 30 to ∞ while fixing the $NaOH/SiO_2$ ratio to 0.33. These data reveal that the phase selectivity of the crystallization can be altered according not only to the length of the dialkyl substituents on the ammonium ion employed, but also to the SiO_2/Al_2O_3 ratio in synthesis mixtures, when ZSM-5 and mordenite, both of which can be synthesized even in the absence of organic SDAs,[2] are not regarded as a result of structure direction exerted by diquaternary cations studied here. While Me_4-diquat-5 gave two different zeolite structures (i.e., nonasil and ZSM-12), depending on the Al content in gels, for example, the Bu_4-diquat-5, Pe_4-diquat-5, or *sec*-Bu_4-diquat-5 ion was found to yield an intergrowth of ZSM-11 (MEL) and ZSM-5 over a specific SiO_2/Al_2O_3 ratio (120). As marked with an arrow in the inset of Figure 1, the powder XRD pattern of the material made using Bu_4-diquat-5 as an organic SDA shows a weak, broad shoulder around $2\theta = 24.5°$, assignable to the (311) reflection of the orthorhombic ZSM-5 material, together with two intense peaks around $2\theta = 23.1$ and 24.0° that correspond to the (501) and (303) reflections of the tetragonal ZSM-11 phase, respectively.[24] A quite similar result was also observed for the XRD pattern of the material prepared with Pe_4-diquat-5 or *sec*-Bu_4-diquat-5. This led us to conclude that all the ZSM-11 materials prepared here are not phase-pure. While ZSM-11 was originally synthesized using tetrabutylammonium (TBA) ion as the organic SDA,[25] a subsequent transmission electron microscopy (TEM) study showed that not only was the material prepared with TBA actually ZSM-11/ZSM-5 intergrowth, but also the synthesis of pure-phase ZSM-11 was quite a difficult task.[26] The fact that Pe_4-diquat-5 and *sec*-Bu_4-diquat-5 can give this intergrowth is somehow unexpected, because tetraalkylammonium cations with pentyl, hexyl, or heptyl groups bulkier than butyl are reported to exclusively crystallize ZSM-5 under the same synthesis conditions.[27] However, we note that the presence of Bu_4-diquat-5, Pe_4-diquat-5, or *sec*-Bu_4-diquat-5 in the synthesis mixture is prerequisite for the crystallization of ZSM-11/ZSM-5 intergrowths even under

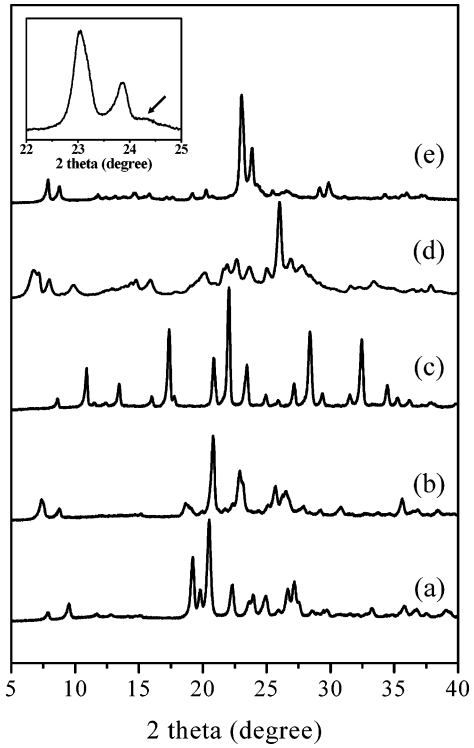

Figure 1. Powder XRD patterns of (a) nonasil, (b) ZSM-12, and (c) levyne prepared with Me_4-diquat-5; (d) MCM-22 prepared with *iso*-Pr_4-diquat-5; and (e) ZSM-11/ZSM-5 prepared with Bu_4-diquat-5. The inset shows the selected region ($2\theta = 22-25°$) of the upper trace. All the zeolites are in their as-made form, and detailed synthesis conditions for these five materials are given in Table 2.

conditions where the gel composition ($SiO_2/Al_2O_3 = 120$ and $NaOH/SiO_2 = 0.33$) is optimized, revealing some degree of their product specificity for the MEL structure. Table 1 also lists the results from syntheses using the eight different $(C_nH_{2n+1})_4$-diquat-5 ions as organic SDAs under the conditions where the $NaOH/SiO_2$ ratio is increased to 0.60 while keeping all other parameters constant. This particular level of Na^+ concentration was selected because it enabled us to obtain ZSM-57, the pure-phase of which has generally been difficult to crystallize even in the presence of Et_6-diquat-5.[7] As seen in Table 1, some of the diquaternary cations studied here brought about significant changes in the phase selectivity of crystallization with increasing $NaOH/SiO_2$ ratio in the synthesis mixture to 0.60. For example, MCM-22 was the product obtained from a sodium aluminosilicate gel with $SiO_2/Al_2O_3 = 30$ containing *iso*-Pr_4-diquat-5 under

(25) Kokotailo, G. T.; Chu, P.; Lawton, S. L.; Meier, W. M. *Nature* **1978**, *275*, 119.
(26) Millward, G. R.; Ramdas, S.; Thomas, J. M.; Barlow, M. T. *J. Chem. Soc., Faraday Trans. 2* **1983**, *79*, 1075.
(27) Gabelica, Z.; Cavez-Bierman, M.; Bordat, P.; Gourgue, A.; Nagy, J. B. *Stud. Surf. Sci. Catal.* **1985**, *24*, 55.

Table 2. Syntheses from Gel Composition $3.0R{\cdot}xNa_2O{\cdot}0.5Al_2O_3{\cdot}30SiO_2{\cdot}1200H_2O$[a,b]

	$NaOH/SiO_2$ ratio in the synthesis mixture							
organic SDA	0.20	0.33	0.47	0.60	0.73	0.87	1.00	1.13
Me_4-diquat-5	amorphous[c]	nonasil	ZSM-12	D + (mordenite)	mordenite	mordenite	mordenite	levyne[d]
Et_4-diquat-5	amorphous[c]	ZSM-5	D + (mordenite)	mordenite	mordenite	mordenite	mordenite	analcime
Pr_4-diquat-5	amorphous[c]	ZSM-5	ZSM-5	ZSM-5	ZSM-5	ZSM-5 + mordenite	mordenite + analcime	P1 + analcime
iso-Pr_4-diquat-5	amorphous[c]	amorphous[c]	MCM-22[c]	ferrierite + (D)	ferrierite	mordenite	mordenite	mordenite
Bu_4-diquat-5	amorphous[c]	ZSM-11/ ZSM-5	ZSM-11/ ZSM-5	ZSM-5	ZSM-5 + (mordenite)	ZSM-5 + mordenite	mordenite + ZSM-5	analcime
iso-Bu_4-diquat-5	amorphous[c]	amorphous[c]	amorphous[c]	D + (mordenite)	D + (mordenite)	mordenite	mordenite + L	analcime
Pe_4-diquat-5	amorphous[c]	ZSM-11/ ZSM-5	ZSM-11/ ZSM-5	ZSM-5	mordenite + ZSM-5	mordenite + ZSM-5	mordenite ZSM-5	analcime
sec-Bu_4-diquat-5	amorphous[c]	amorphous[c]	amorphous[c]	ZSM-5 + mordenite	D + (mordenite)	L + mordenite	mordenite	mordenite + P1

[a] R is organic SDA and x is varied between $3.0 \le x \le 17.0$. The crystallization conditions are the same as those given in Table 1, unless otherwise stated. [b] The phase appearing first is the major product, and the phase obtained in a trace amount is given in parentheses. D and L are dense (mainly quartz) and layered phases, respectively. [c] The material obtained after 14 days of heating at 433 K. [d] The material obtained after 3 days of heating at 433 K.

Table 3. Chemical Compositions for the Representative Zeolites Prepared in This Study

zeolite	unit cell composition[a]	Si/Al ratio	BET surface area,[b] $m^2\,g^{-1}$
nonasil	$(Me_4\text{-diquat-5})_{3.0}Na_{0.4}Al_{2.6}Si_{85.4}O_{176}{\cdot}3.3H_2O$	33	[c]
ZSM-12	$(Me_4\text{-diquat-5})_{1.8}Na_{0.5}Al_{1.0}Si_{55}O_{112}{\cdot}4.8H_2O$	55	310
levyne	$(Me_4\text{-diquat-5})_{3.9}Na_{2.3}Al_{6.1}Si_{47.9}O_{108}{\cdot}5.6H_2O$	7.9	612
MCM-22	$(iso\text{-}Pr_4\text{-diquat-5})_{2.6}Na_{2.0}Al_{4.3}Si_{67.7}O_{144}{\cdot}8.7H_2O$[d]	16	432
ZSM-11/ZSM-5	$(Bu_4\text{-diquat-5})_{2.3}Na_{0.2}Al_{0.8}Si_{95.2}O_{192}{\cdot}6.2H_2O$	119	432
ZSM-11/ZSM-5	$(sec\text{-}Bu_4\text{-diquat-5})_{2.0}Na_{0.3}Al_{0.7}Si_{95.3}O_{192}{\cdot}7.7H_2O$	136	380

[a] Determined from a combination of elemental and thermal analyses. All the occluded organic SDAs are assumed to be counterbalanced by framework negative charges. [b] Determined from N_2 adsorption data for the proton form of each zeolite. [c] Not determined. [d] The material is assumed to crystallize as the so-called MWW structure rather than its lamellar precursor.

high NaOH conditions. In addition, any of Bu_4-diquat-5, Pe_4-diquat-5, and *sec*-Bu_4-diquat-5 did not direct the crystallization of ZSM-11/ZSM-5 intergrowths, which is in contrast to the trend found in the synthesis at a lower $NaOH/SiO_2$ ratio (0.33).

To examine more closely the effects of the NaOH content on the final product in synthesis mixtures containing $(C_nH_{2n+1})_4$-diquat-5 ions with $n = 1-5$, we have varied the $NaOH/SiO_2$ ratio in the gel from 0.20 to 1.13 and performed zeolite syntheses under conditions where the SiO_2/Al_2O_3 ratio is fixed at 60. The synthesis results in Table 2 reveal that at $NaOH/SiO_2$ ratios up to 1.00, this group of diquaternary cations produces no zeolitic phases other than those already given in Table 1. When the $NaOH/SiO_2$ ratio in the gel was increased to 1.13, however, the phase formed with Me_4-diquat-5 was levyne, a product that has previously been reported to crystallize only using polycyclic organic SDAs with a high degree of conformational rigidity.[12−17] While the synthesis procedure for MCM-22 with *iso*-Pr_4-diquat-5 described above proved to be highly reproducible, on the other hand, the SiO_2/Al_2O_3 ratio range yielding its pure form was found to be very narrow (Table 1). This is also the case for the synthesis of levyne in the presence of Me_4-diquat-5, since we always obtained a mixture of analcime or quartz and this small-pore zeolite when using gels with $SiO_2/Al_2O_3 < 40$ or > 60. It thus appears that a reasonable amount of lattice charge is needed in the synthesis mixture, together with a certain level of Na^+ concentration, to synthesize MCM-22 and levyne using *iso*-Pr_4-diquat-5 and Me_4-diquat-5, respectively. However, we found that when the eight different $(C_nH_{2n+1})_4$-diquat-5 ions with $n = 1-5$ were replaced by the corresponding $(C_nH_{2n+1})_2$-diquat-5 ions formed of two monoalkylammonium groups connected by a pentamethylene bridging unit, the zeolitic products crystallized from synthesis mixtures with a wide range of oxide compositions given in Tables 1 and 2 were always from ZSM-5, ferrierite, and mordenite.[28] This suggests that the phase selectivity of the crystallization in the presence of linear diquaternary alkylammonium ions can be sensitive to both the bulkiness and length of the groups on the ammonium ion, despite their highly flexible nature which allows them to undergo a large number of conformational variations under the zeolite synthesis conditions.

Figure 1 shows the powder XRD patterns of the representative zeolites prepared in this study. Comparison with the XRD patterns in the literature[24] reveals that each material is highly crystalline and no reflections other than those from the corresponding structure are observed. This is particularly true in the case of levyne, since its proton form (i.e., H-levyne) exhibits a very high BET surface area of over 600 $m^2{\cdot}g^{-1}$ (Table 3). The SEM micrograph (not shown) of this small-pore material shows that it appears as agglomerates of heavily overlapped rhombic crystals of $0.5-3.0\ \mu m$, which is somewhat different from the morphology reported previously.[29−31] The chemical compositions of selected

(28) Han, B.; Lee, S.-H.; Shin, C.-H.; Hong, S. B. Unpublished.
(29) Tuoto, C. V.; Regina, A.; Nagy, J. B.; Nastro, A. *Microporous Mesoporous Mater.* **1998**, *20*, 247.
(30) Caullet, P.; Delmotte, L.; Faust, A. C.; Guth, J. L. *Zeolites* **1995**, *15*, 139.

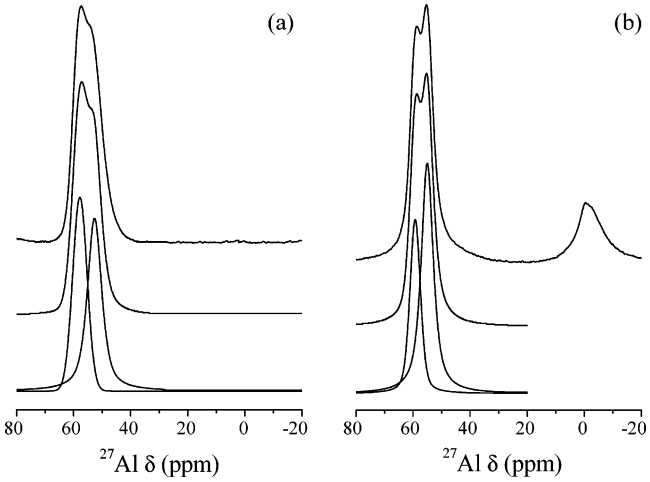

Figure 2. ^{27}Al MAS NMR spectra of the (a) as-made and (b) proton forms of levyne obtained using Me_4-diquat-5: experimental (top), simulated (middle), deconvoluted components (bottom).

zeolites in their as-made form, which were determined from a combination of elemental and thermal analyses, are given in Table 3. A considerable imbalance between the amount of Al and the sum of organic and Na^+ ions compensating for framework negative charges is observed for all six zeolites. This suggests that a part of the dialkylammonium groups of the organic SDAs occluded within these materials exists in the form of bromide or hydroxide to serve as space-filling species rather than as charge-compensating cations. An alternative explanation is the presence of connectivity defects that afford $Si-O^-$ groups to counter-balance the occluded diquaternary cations, as frequently found in the high- and pure-silica zeolites synthesized with organic SDAs in alkaline media.[32]

Figure 2 shows the ^{27}Al MAS NMR spectra of the as-made and proton forms of levyne prepared here, together with the simulated spectra and their deconvoluted components. As-made levyne exhibits two tetrahedral ^{27}Al resonances around 53 and 58 ppm. The same result was also observed for H-levyne, although these two resonances are shifted slightly downfield relative to the as-made material. This indicates the presence of two crystallographically distinct tetrahedral Al sites in levyne, which is consistent with its known structure.[12] We note here that any of the reported ^{27}Al MAS NMR spectra of levyne zeolites with different Si/Al ratios (6.5−20) has not been clearly resolved into two components in the framework tetrahedral region.[29−31] We believe that this is mainly due to notable differences in the shape, size, and C/N^+ value of the organic SDA used in our synthesis and of known organic additives yielding LEV-type materials. In fact, it has been suggested that the Al distribution pattern in real zeolites with multiple tetrahedral sites (T-sites) can be affected by the charge distribution of the organic species used in their syntheses.[33,34] When using

Table 4. Chemical Shifts and Relative Intensities of the ^{27}Al MAS NMR Resonances of the As-Made and Proton Forms of Levyne Prepared Here

		Al species						
		Al_1(4Si)		Al_2(4Si)		octahedral Al		
zeolite	Si/Al	δ (ppm)	*I* (%)	δ (ppm)	*I* (%)	δ (ppm)	*I* (%)	*I* (Al_1)/ *I* (Al_2)
as-made levyne	7.9	57.9	56	52.6	44			1.27
H-levyne	7.9	59.3	27	55.1	52	−1.9	21	0.52

the equation of Lippmaa et al.,[35] the average Al−O−Si angles for the uncorrected high- and low-field ^{27}Al resonances from as-made levyne were calculated to be 148.2 and 158.8°, respectively. These values are in good agreement with the average T_1−O−T and T_2−O−T angles (148.5 and 155.5°, respectively) derived from the Rietveld refinement of the synchrotron powder XRD data for an as-made pure-silica levyne obtained in the presence of *N*-methylquinuclidinium ions,[12] despite the empirical nature of the relationship proposed by Lippmaa et al. and the notable difference in Si/Al ratios for the two materials compared here. A quite similar result was also observed for H-levyne. Therefore, the high- and low-field tetrahedral ^{27}Al NMR resonances in Figure 2 can be assigned to Al atoms in sites T_1 and T_2 with multiplicities of 36:18 of the LEV framework, respectively.

Table 4 summarizes results obtained from curve deconvolution of the ^{27}Al MAS NMR spectra in Figure 2. Notice that the relative intensity ratio (1.3:1.0) of the two ^{27}Al resonances from as-made levyne is considerably smaller than the ideal value (2:1) expected for the statistical distribution of Al atoms over the two sites T_1 and T_2 with the so-called Loewenstein's rule, which is indicative of preferential Al substitution into the low-multiplicity site during the crystallization process. The second-order quadrupolar interaction gives rise to asymmetric line broadenings and line shifts but is inversely proportional to the magnetic field strength, which is the main impetus for recording the MAS NMR spectra of quadrupolar nuclei like ^{27}Al at as a high magnetic field strength as possible. Considering the strength (11.7 T) of the magnetic field employed in our ^{27}Al MAS NMR experiments, the line-broadening influence of the second-order quadrupolar interaction on the spectrum of as-made levyne, and hence the degree of uncertainty in the intensity ratio of the deconvoluted components, may not be so large as to afford an ideal intensity ratio of 2:1 for this small-pore material. If such is the case, levyne could then be added to the growing list of zeolites where the spatial distribution of Al atoms over the available tetrahedral sites proved to be nonrandom.[36−41] There is one published ^{27}Al MQ MAS NMR

(31) De Luca, P.; Violante, D.; Vuono, D.; Catanzaro, L.; Nagy, J. B.; Nastro, A. *Microporous Mesoporous Mater.* **2004**, *71*, 39.
(32) Engelhardt, G.; Michel, D. *High-Resolution Solid State NMR of Silicates and Zeolites*; Wiley: Chichester, 1987.
(33) Shantz, D. F.; Fild, C.; Koller, H.; Lobo, R. F. *J. Phys. Chem. B* **1999**, *103*, 10858.
(34) Sabater, M. J.; Sastre, G. *Chem. Mater.* **2001**, *12*, 4520.
(35) Lippmaa, E.; Somoson, A.; Mägi. M. *J. Am. Chem. Soc.* **1986**, *108*, 1730.
(36) Klinowski, J.; Anderson, M. W.; Thomas, J. M. *J. Chem. Soc., Chem. Commun.* **1983**, 525.
(37) Schmitt, K. D.; Kennedy, G. J. *Zeolites* **1994**, *14*, 635.
(38) Lawton, S. L.; Fung, A. F.; Kennedy, G. J.; Alemany, L. B.; Chang, C. D.; Hatzikos, G. H.; Lissy, D. N.; Rubin, M. K.; Timken, H.-K. C.; Steuernagel, S.; Woessner, D. E. *J. Phys. Chem.* **1996**, *100*, 3788.
(39) Han, O. H.; Kim, C.-S.; Hong, S. B. *Angew. Chem., Int. Ed.* **2002**, *41*, 469.
(40) Kennedy, G. J.; Afeworki, M.; Hong, S. B. *Microporous Mesoporous Mater.* **2002**, *52*, 55.
(41) Abraham, A.; Lee, S.-H.; Shin, C.-H.; Hong, S. B.; Prins, R.; van Bokhoven, J. A. *Phys. Chem. Chem. Phys.* **2004**, *6*, 3031.

study showing that the Al distribution in levyne with Si/Al = 15 is random.[42] The discrepancy with our results appears to be due to differences in the Si/Al ratio of the respective samples, since the preference of Al atoms for particular T-sites in as-made zeolites such as ZSM-5 and beta differs significantly according to the Si/Al ratio in synthesis mixtures and thus is kinetic in nature.[39,41] As shown in Figure 2 and Table 4, on the other hand, the spectrum of H-levyne contains three signals: two corresponding to tetrahedral Al and a broad resonance around −2 ppm attributable to octahedral Al in the relative intensity ratio 0.5:1.0:0.4, respectively. Since no special care was taken to normalize the weight of samples used in recording the ^{27}Al MAS NMR spectra in Figure 2, we cannot unambiguously ensure that all Al in H-levyne is detected in the spectrum and no intensity loss is caused by the presence of severely distorted octahedral Al frequently referred to as "NMR invisible" species.[32] Compared to the limited accuracy of the intensity from octahedral species, however, the relative intensity (0.5:1.0) of the two tetrahedral ^{27}Al resonances from H-levyne may be reliable. In the case of the LEV topology, three O−T−O bonds of T_1 are constrained within 4-rings, while in T_2 only two O−T−O bands are in such a situation.[43] Since the strain on the former site is, in principle, larger than that on the latter one, it is clear that the extent of dealumination in levyne caused by the initial calcination at 823 K to remove the occluded organic SDA and the subsequent NH_4^+ ion exchange and calcination steps is much higher on the Al atoms in site T_1 than those in site T_2, unlike the case of Al substitution in the same zeolite framework.

Figure 3 shows the ^{1}H−^{13}C CP MAS NMR spectra of as-made nonasil, ZSM-12, and mordenite, and levyne, all of which were prepared using the same organic SDA, i.e., Me_4-diquat-5, together with the spectrum of the dibromide salt of this diquaternary cation, energy-minimized in a packed crystalline organic solid. The assignments of the observed resonances are also indicated in Figure 3, and their chemical shifts are given in Table 5. These data clearly show that Me_4-diquat-5 remains intact upon its occlusion into the pores of each zeolite and has not decomposed under the crystallization conditions. However, there are small but nonnegligible differences in the ^{13}C chemical shift, which must be closely related to changes in the conformation of the occluded cation and in its interactions with the zeolite frameworks. When Me_4-diquat-5 is located inside the cages of nonasil, for example, the resonance of its methyl carbon is observed at 53.9 ppm and thus is shifted downfield relative to the corresponding carbon resonance of the solid-state dibromide salt appearing at 50.9 ppm. This is also the case for the resonance of the methylene carbons bonded to the nitrogen. The NON structure contains three different types of cages: nonahedral [$4^1 5^8$], octahedral [$5^4 6^4$], and icosahedral [$5^8 6^{12}$] units.[43] While the first two cages must be too small to host Me_4-diquat-5, the effective dimensions of the third one are approximately 8.9 × 7.1 × 7.1 Å. Energy minimization

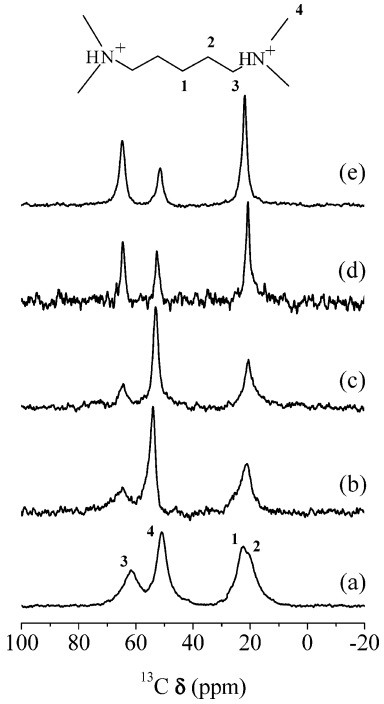

Figure 3. ^{1}H−^{13}C CP MAS NMR spectra of (a) Me_4-diquat-5 dibromide salt and as-made (b) nonasil, (c) ZSM-12, (d) mordenite, and (e) levyne, showing the assignment of each resonance.

Table 5. ^{1}H−^{13}C CP MAS NMR Chemical Shift Data for Me_4-diquat-5[a]

	chemical shift, ppm from TMS			
sample	C_1	C_2	C_3	C_4
Me_4-diquat-5·2Br	20.9	22.5	61.7	50.9
nonasil	21.1		64.6	53.9
ZSM-12	20.5		64.3	53.0
mordenite	20.6		64.5	52.2
levyne	21.7		64.6	51.3

[a] The assignments of each resonance of Me_4-diquat-5 are the same as those given in Figure 3. C_1 and C_2 carbon resonances of this cation overlap in these four zeolites.

calculations reveal that the best model for free Me_4-diquat-5 that does not violate any geometric constraints has approximate dimensions of 12.0 × 6.1 × 6.1 Å. Thus, the largest dimension of the NON cage is shorter by ∼3 Å than the length of free Me_4-diquat-5. This suggests that a certain degree of spatial constraints should be imposed on the encapsulated diquaternary cation, which is responsible for the observed shift of its carbon resonances to lower field. A similar interpretation can also be made for the ^{1}H−^{13}C CP MAS NMR spectra of the organic guest molecules in ZSM-12 and mordenite. The pore dimension (5.6 × 6.0 Å) of straight 12-ring channels in the former zeolite is slightly smaller than the approximate cross section (6.1 × 6.1 Å) of free Me_4-diquat-5, whereas the opposite holds for the analogous channels (6.5 × 7.0 Å) in the latter zeolite. Therefore, it is not very difficult to predict that the degree of geometric constraints and van der Waals interactions of the occluded Me_4-diquat-5 with the zeolite framework could be higher in ZSM-12 than in mordenite. This explains why the methyl carbon resonance of the organic in ZSM-12 is shifted slightly downfield relative to that of as-made mordenite (Table 5). On the other hand, if the heptadecahedral [$4^9 5^6 8^3$] LEV cage in levyne retains only one Me_4-diquat-5

(42) Lentz, P.; Nagy, J. B.; Delevoye, L.; Dumazy, Y.; Fernandez, C.; Amoureux, J.-P.; Tuoto, C. V.; Nastro, A. *Colloids Surf. A* **1999**, *158*, 13.
(43) International Zeolite Association, Structure Committee, http://www.iza-structure.org.

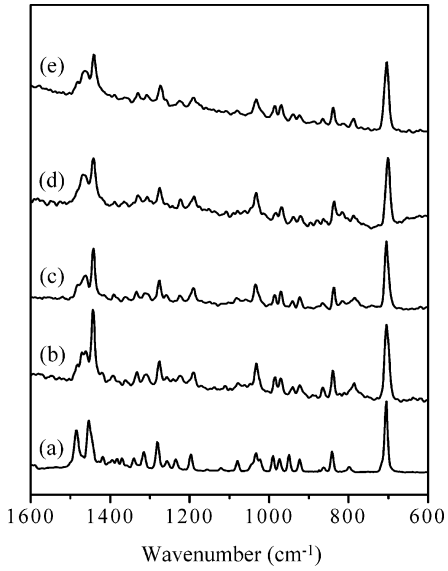

Figure 4. Raman spectra in the 600−1600 cm^{-1} region of (a) 0.5 M aqueous solution of Me_4-diquat-5 dibromide and as-made (b) nonasil, (c) ZSM-12, (d) mordenite, and (e) levyne with Me_4-diquat-5 occluded in their pores.

molecule, the methyl carbon resonance of the encapsulated organic should shift to lower field relative to that from as-made nonasil. This is because the approximate dimensions (7.3 × 6.3 × 6.3 Å) of the LEV cage are considerably smaller than those (8.9 × 7.1 × 7.1 Å) of the NON cage. As seen in Figure 3 and Table 5, however, the chemical shift (51.3 ppm) of the methyl carbon resonance of as-made levyne was found to be nearly the same as that (50.9 ppm) observed for the dibromide salt, indicating that the methyl groups of the occluded diquaternary cation do not experience severe geometric constraints and van der Waals interactions with the zeolite framework. Therefore, we suggest that the organic guest molecule in levyne spans across two LEV cages, which can be further supported by computer modeling results (see below).

Figure 4 shows the Raman spectra in the 600−1600 cm^{-1} region of as-made nonasil, ZSM-12, mordenite, and levyne. The Raman spectrum of Me_4-diquat-5 in aqueous solution is also given in Figure 4. In agreement with the $^1H-^{13}C$ CP MAS NMR data given above, it is clear that Me_4-diquat-5 not only remains intact inside the pores of each zeolite host, but also exhibits a noticeable change in the band position of its specific skeletal Raman vibration modes. When compared with the Raman spectra of various tetraalkylammonium salts in the literature,[44] the band appearing at 1454 cm^{-1} in the Raman spectrum of free Me_4-diquat-5 can be tentatively assigned to the CH_3 asymmetric deformation mode. As shown in Figure 4, however, all the four zeolites containing Me_4-diquat-5 as a guest molecule give this deformation at 1442−1444 cm^{-1}. Despite its red-shift relative to the corresponding vibration mode of Me_4-diquat-5 in aqueous solution, therefore, the CH_3 asymmetric deformation band appears to be insensitive to notable differences in the pore structure of zeolites within which the organic molecules are occluded. A quite similar trend was also observed for the symmetric C−N stretching mode appearing at 705 cm^{-1} in the Raman spectrum of free Me_4-diquat-5, since no detectable

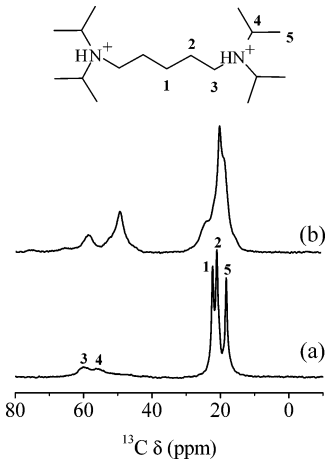

Figure 5. $^1H-^{13}C$ CP MAS NMR spectra of (a) *iso*-Pr_4-diquat-5 dibromide salt and as-made (b) MCM-22, showing the assignment of each resonance.

differences in its band position and intensity are caused by the occlusion of Me_4-diquat-5 into the zeolite pores. While these results contrast with those found in the Raman spectra of the slightly bulkier Me_6-diquat-5 molecules in various zeolites such as ZSM-48, ZSM-12, and MCM-22,[11] the precise reason Raman spectroscopy is not sensitive enough to illustrate the effects of the confined space around the Me_4-diquat-5 molecules is not known at this time.

Figure 5 shows the $^1H-^{13}C$ CP MAS NMR spectra of as-made MCM-22 and *iso*-Pr_4-diquat-5 dibromide salt. Although the intensities of the ^{13}C resonances are not quantitative due to differences in their cross polarization dynamics, it appears that all the carbon atoms of the occluded *iso*-Pr_4-diquat-5 molecule can be observed using this experiment. As seen in Figure 5, however, as-made MCM-22 shows signs of four components in the chemical shift region 15−25 ppm where three resonances, due to the methyl carbon in the *iso*-propyl groups and the second and third methylene carbons in the central pentyl chain, should be otherwise observed. This suggests that more than one degree of geometric constraints and van der Waals interactions with the zeolite surface is imposed on the occluded *iso*-Pr_4-diquat-5. Because of the heavily overlapped feature of the ^{13}C resonances in the region 15−25 ppm, however, the origin of the appearance of a new resonance in this region is at present not understood. Figure 5 also shows that the resonances at 49.3 and 58.6 ppm, which are assigned to methylyne and methylene carbons bonded to the nitrogen of the occluded diammonium ion, respectively, are shifted considerably upfield relative to those of the pure dibromide salt. The MWW structure consists of two independent 10-ring channels: one formed by two-dimensional sinusoidal channels (4.1 × 5.1 Å), and the other by large supercages (7.1 Å in diameter and 18.2 Å in height) that can be accessible through 10-ring widows only.[43] Although detailed information on the locations and conformations of *iso*-Pr_4-diquat-5 in as-made MCM-22 pores cannot be obtained from the $^1H-^{13}C$ CP MAS NMR spectra in Figure 5, we speculate that the observed spectral changes are characteristic of the

(44) Lin-Vien, D.; Colthup, N. B.; Fateley, W. G.; Grasselli, J. G. *Handbook of Infrared and Raman Characteristic Frequencies of Organic Molecules*; Academic: San Diego, CA, 1991.

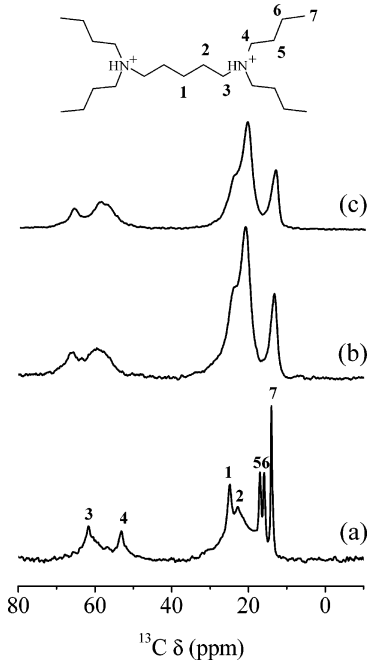

Figure 6. $^1H-^{13}C$ CP MAS NMR spectra of (a) Bu_4-diquat-5 dibromide salt and as-made (b) ZSM-11/ZSM-5 and (c) ZSM-5, showing the assignment of each resonance.

conformation adopted by this doubly charged cation inside the supercages rather than inside the sinusoidal 10-ring channels. This is because the pore dimension of the sinusoidal channels in MCM-22 is considerably smaller than the diameter (>7 Å) of the di-*iso*-propylammonium moieties of *iso*-Pr_4-diquat-5. As expected, on the other hand, the Raman spectra (not shown) of *iso*-Pr_4-diquat-5 in aqueous solution and as-made MCM-22 were found to be quite similar to each other. Like the case of the occluded Me_4-diquat-5 in Figure 4, however, there is a red-shift of the CH_3 asymmetric deformation band (1463 cm^{-1} for free *iso*-Pr_4-diquat-5; 1452 cm^{-1} for as-made MCM-22).

Figure 6 compares the $^1H-^{13}C$ CP MAS NMR spectrum of the Br_4-diquat-5 dibromide salt with the spectra of as-made ZSM-11/ZSM-5 and ZSM-5. Like the trend found in Figures 3 and 5, there are notable changes in the position of the ^{13}C resonances of Bu_4-diquat-5 after its encapsulation within the pores of ZSM-11/ZSM-5 and ZSM-5. For example, two resonances of the second and third methylene carbons in the butyl groups appearing around 17 and 16 ppm in the solid-state spectrum of the dibromide salt are no longer observed in the analogous region of the $^1H-^{13}C$ CP MAS NMR spectrum of Bu_4-diquat-5 in ZSM-11/ZSM-5 or ZSM-5. Furthermore, in contrast to the case of TBA ions in ZSM-11,[45] no splitting of the methyl resonance is found. However, Figure 6 shows that both the as-made ZSM-11/ZSM-5 and ZSM-5 materials give essentially the same spectral changes, probably due to the structural analogy between the MFI and MEL topologies. The Raman spectra of these two materials together with the spectrum of Br_4-diquat-5 in aqueous solution are given in Figure 7. The Raman signature of the occluded organic molecules includes red-shift of the symmetric and asymmetric C−N stretching

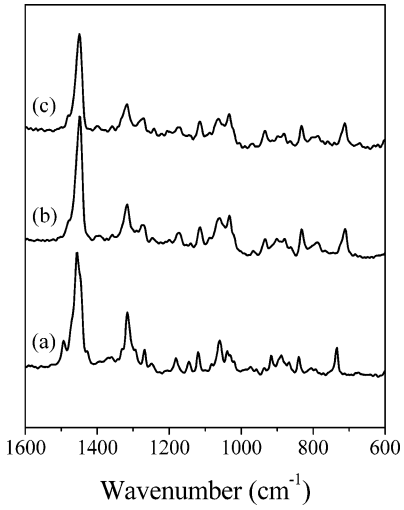

Figure 7. Raman spectra in the 600−1600 cm^{-1} region of (a) 0.5 M aqueous solution of Bu_4-diquat-5 dibromide and as-made (b) ZSM-11/ZSM-5 and (c) ZSM-5 with Bu_4-diquat-5 occluded in their pores.

and CH_3 asymmetric deformation bands observed at 734, 841, and 1456 cm^{-1} for Bu_4-diquat-5 in aqueous solution, respectively. Also, there are notable differences in the band position and intensity of the C−C stretching mode at 1040−1100 cm^{-1} and the CH_2 wagging mode at 1300−1350 cm^{-1}. As shown in Figure 7, however, no spectral differences are observed for as-made ZSM-11/-ZSM-5 and ZSM-5. This again confirms that the Bu_4-diquat-5 molecules in these two materials adopt conformations which are quite similar to each other, but are different from the conformation of the free organic molecule.

The detailed crystal structures of nonasil, ZSM-12, mordenite, and levyne, all of which can now be synthesized using the same organic SDA, i.e., Me_4-diquat-5, are currently available in the literature.[24] To gain further information concerning the host−guest interactions occurring within these four materials, therefore, we have attempted to optimize the locations and conformations of the occluded Me_4-diquat-5 molecules via energy minimization calculations as mentioned earlier. The lowest-energy conformations for Me_4-diquat-5 within the structures of nonasil, ZSM-12, mordenite, and levyne are shown in Figure 8. It can be seen that Me_4-diquat-5 fits into the isolated small NON cage in nonasil by adopting an "S-shaped" conformation. Figure 8 also shows that this organic molecule matches well with the undulations in both the ZSM-12 and mordenite 12-ring pores. By contrast, the molecule in levyne was found to span across two LEV cages through the 8-ring window. On the basis of the dimensions of the free Me_4-diquat-5 molecule and the NON and LEV cages given above, their approximate volumes can be calculated with Marler's method[46] to be 234, 235, and 152 $Å^3$, respectively. This suggests that the organic SDA needs to adopt the "S-shaped" conformation to fit tightly within the NON cage. Although its flexibility clearly contributes to its ability to direct the formation of nonasil, the energy required to adopt this conformation is more than offset by the increased van der Waals interactions with the zeolite framework caused by such a tight fit. The tight

(45) Nagy, J. B.; Gabelica, Z.; Derouane, E. G. *Zeolites* **1983**, *3*, 43.

(46) Marler, B. Ph.D. Thesis, Universität Kiel, 1989.

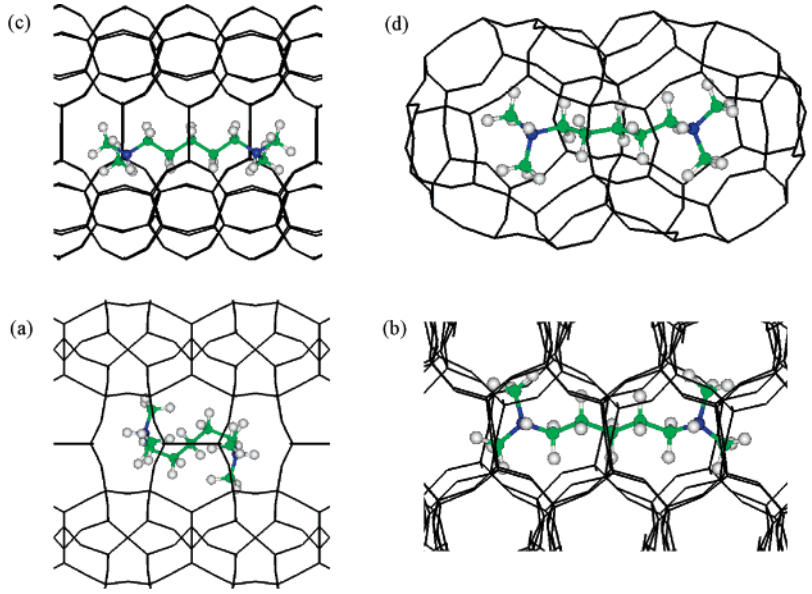

Figure 8. Energy-minimized conformations of the Me_4-diquat-5 molecule within the frameworks of (a) nonasil, (b) ZSM-12, (c) mordenite, and (d) levyne.

encapsulation of Me_4-diquat-5 within the NON cage is consistent with the results obtained using $^1H-^{13}C$ CP MAS NMR spectroscopy. Since the volume of the LEV cage is too small to accommodate a single Me_4-diquat-5, on the other hand, the molecule must span two cages. This means that Me_4-diquat-5 may fit less tightly within the LEV cage than within the NON cage, leading to fewer unfavorable interactions in the former cage. As a consequence, there appears to be no need for a significant conformational rearrangement of the occluded molecule in levyne, explaining why its methyl carbon resonance is essentially unchanged relative to the Me_4-diquat-5 dibromide salt (Table 5). Computer simulation also predicts a maximum filling of 3 Me_4-diquat-5 ions per unit cell of this small-pore material, which is considerably smaller than the value (3.9) determined from TGA/DTA (Table 3). This discrepancy is not unexpected because the exothermic weight losses in TGA/DTA were assumed to originate from the combustion of organic species balancing only framework negative charges. In fact, elemental analysis has revealed that the total organic content is 11.1 wt % (C, 7.44; H, 1.75; N, 1.90), giving a number of 2.8 organic SDA molecules per unit cell. Prior to this work on the Me_4-diquat-5 in levyne, to our knowledge, tetramethylethylenediamine in ZSM-39[47] was the only known case in which a single organic molecule used as an SDA in zeolite synthesis occupies more than one zeolite cage. The stabilization energies determined by calculating the difference in energies of the free Me_4-diquat-5 molecule and the molecule occluded within four different zeolite frameworks are listed in Table 6. These data reveal that while the stabilization energy per mole T-atoms decreases in the order levyne $\approx$ nonasil > mordenite > ZSM-12, the framework-molecule interaction energies per mole SDA within the frameworks of the last three zeolites are similar to one another and are slightly lower than the value calculated for the molecule within the first zeolite. This suggests that the Me_4-diquat-5 molecules occluded can adapt distinct conformations to yield a good geometric match and a high space-filling, depending on the structural aspects of each zeolite host, which must be a consequence of their highly flexible nature. Therefore, it is most likely that Me_4-diquat-5 may play a generally beneficial but structurally nonspecific space-filling role in the crystallization of these four zeolites.

Table 6. Stabilization Energies Calculated for the Me_4-diquat-5 Cation within the Pores of Various Zeolites

zeolite host	no. of SDA molecules/ unit cell	stabilization energy, kJ mol^{-1} SDA	no. of T-atoms/ unit cell	stabilization energy, kJ mol^{-1} T-atoms
nonasil	4	−111.9	88	−5.09
ZSM-12	2	−116.7	56	−4.17
mordenite	2	−109.3	48	−4.55
levyne	3	−92.3	54	−5.13

Since structural data on as-made MCM-22, a lamellar precursor that undergoes dehydroxylation upon calcinations between the layered sheets to generate the so-called MWW structure, remain unknown, it is not currently possible to undertake molecular modeling studies on the occluded *iso*-Pr_4-diquat-5 in this phase. While this also appears to be the case for Bu_4-diquat-5, Pe_4-diquat-5, and *sec*-Bu_4-diquat-5 in ZSM-11/ZSM-5 intergrowths, due to the lack of information on their MFI-MEL twin fault densities, the energy minimization calculations on the Bu_4-diquat-5 molecules with different levels of concentration inside the frameworks of ZSM-11 and ZSM-5 allow us to gain some insight into the origin of the intergrowth formation. We note that the SDA molecule in each case spans across two channel intersections, as shown in Figure 9. At a low SDA concentration (one molecule per 2 × 2 × 2 unit cells) the nonbonded energy (−251.9 kJ mol^{-1} SDA) obtained for Bu_4-diquat-5 in ZSM-5 was calculated to be significantly more favorable than that (−231.1 kJ mol^{-1} SDA) in ZSM-11. As the number of SDA molecules per 2 × 2 × 2 unit cells increases from one to four, however, the binding energy becomes much less favorable in ZSM-5 (−226.6 kJ mol^{-1} SDA). This can be

(47) Tang, X.; Sun, Y.; Wu, T.; Wang, L.; Fei, L.; Long, Y. *J. Chem. Soc., Faraday Trans.* **1993**, *89*, 1839.

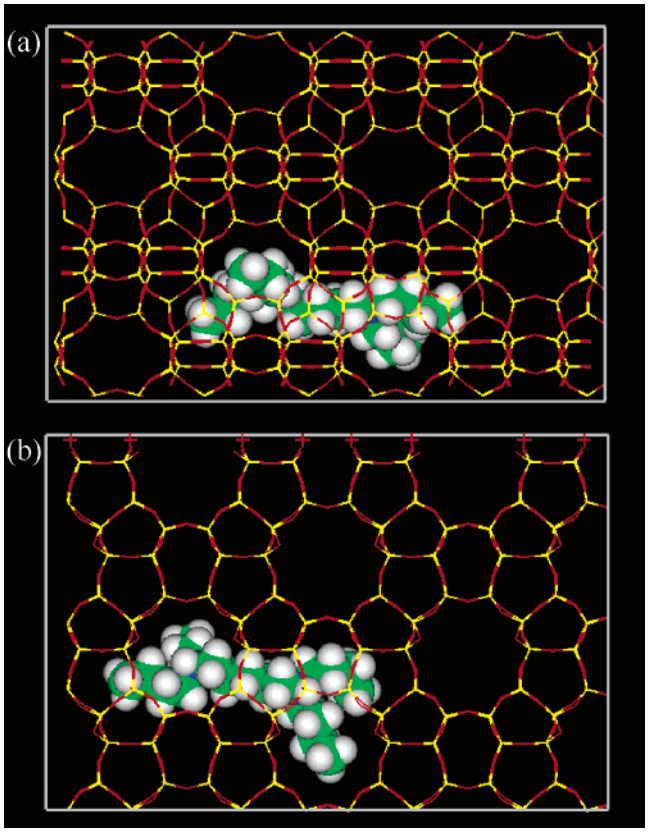

Figure 9. Energy-minimized locations for Bu_4-diquat-5 inside (a) ZSM-5 and (b) ZSM-11.

rationalized by considering that the butyl groups in adjacent Bu_4-diquat-5 molecules become closer together at high SDA concentration levels, leading to a decrease in nonbonded energy. Although the total binding energy at a higher loading is still more favorable in ZSM-5, by contrast, the change (12.9 kJ mol^{-1} SDA) in the nonbonded energy (−218.2 kJ mol^{-1} SDA) for Bu_4-diquat-5 within ZSM-11 was found to be much smaller than that (25.3 kJ mol^{-1} SDA) observed for ZSM-5. This indicates that interactions between adjacent organic SDAs favor the formation of ZSM-11. As shown diagrammatically in Figure 10, therefore, we propose that the central $N^+(CH_2)_5N^+$ chain of Bu_4-diquat-5 could contribute mainly to the crystallization of ZSM-5, while the ZSM-11 formation may be favored when the butyl groups from adjacent molecules appropriately align. If such is the case, both structures could readily form their intergrowths. Regardless of the reliability of the proposal given above, however, it is appears that like the case of Me_4-diquat-5, the structurally nonspecific space-filling role may also be a general characteristic of Bu_4-diquat-5. This is because the

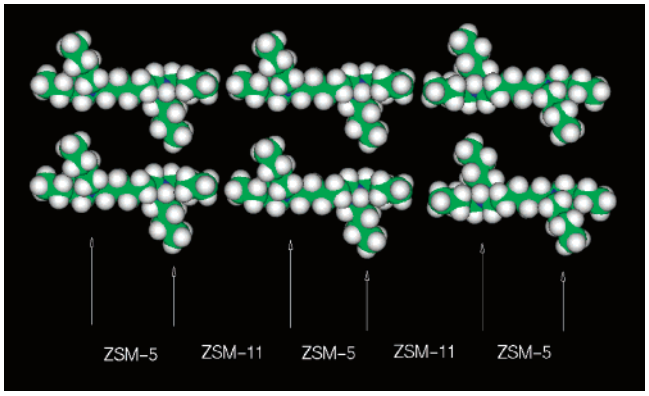

Figure 10. Schematic diagram showing a possible mechanism by which the Bu_4-diquat-5 molecules may lead to the ZSM-11/ZSM-5 intergrowth formation.

oxide composition range yielding pure ZSM-5 or ZSM-11/ZSM-5 in the presence of this diquaternary cation is very narrow (Table 1).

Conclusions

The overall synthesis results of this study demonstrate that the phase selectivity of zeolite syntheses in the presence of flexible $(C_nH_{2n+1})_2HN^+(CH_2)_5N^+H(C_nH_{2n+1})_2$ ions with $n = 1-5$ is sensitive to the Al and alkali cation contents in synthesis mixtures, as well as to the length of the dialkyl groups on the ammonium ion used. Among the organic SDAs studied here, the most diverse phase selectivity was observed for Me_4-diquat-5 yielding nonasil, ZSM-12, mordenite, and levyne. By contrast, the *iso*-Pr_4-diquat-5 ion was found to produce MCM-22, when the concentrations of inorganic components in the synthesis mixture are properly selected. The ^{27}Al MAS NMR results indicate that both the Al substitution and dealumination patterns in levyne prepared here are nonrandom. Analysis of the $^1H-^{13}C$ CP MAS NMR and Raman spectra obtained from the Me_4-diquat-5 molecules occluded in four different zeolites reveals that the conformations of the occluded organic molecules are distinctly different from one another, which has been further confirmed by computer modeling studies.

Acknowledgment. Funding for this work was provided by the Korea Science and Engineering Foundation (R02-2003-000-10087-0) and the Korea Energy Management Corporation R&D Management Center for Energy and Resources (2003-C-NA03-P-02-0-000-2003). We thank Dr. S. W. Nam of KIST for elemental analysis. We also thank one anonymous reviewer for the valuable comments and discussions.

CM048418+